Neuropeptides 59 (2016) 97–109

Contents lists available at ScienceDirect

Neuropeptides

journal homepage: www.elsevier.com/locate/npep

Temperature dependence of the control of energy homeostasis requires CART signaling

Jackie Lau, Yan-Chuan Shi *,[1], Herbert Herzog *,[1]

Neuroscience Division, Garvan Institute of Medical Research, St Vincent's Hospital, Sydney 2010, Australia
Faculty of Medicine, UNSW Australia, Sydney 2052, Australia

ARTICLE INFO

Article history:
Received 7 January 2016
Received in revised form 22 March 2016
Accepted 31 March 2016
Available online 5 April 2016

Keywords:
CART
Thermoneutrality
Energy homeostasis
BAT
Mild cold exposure

ABSTRACT

Cocaine- and amphetamine-regulated transcript (*CART*) is a key neuropeptide with predominant expression in the hypothalamus central to the regulation of diverse biological processes, including food intake and energy expenditure. While there is considerable information on CART's role in the control of feeding, little is known about its thermoregulatory potential. Here we show the consequences of lack of CART signaling on major parameters of energy homeostasis in *CART*$^{-/-}$ mice under standard ambient housing (RT, 22 °C), which is considered a mild cold exposure for mice, and thermoneutral conditions (TN, 30 °C). WT mice kept at RT showed an increase in food intake, energy expenditure, BAT UCP-1 expression, and physical activity compared with TN condition, reflecting the augmented energy demand for thermogenesis at RT. On the molecular level, RT housing led to upregulated mRNA expression of *TH*, *CRH*, and *TRH* at the PVN, while *NPY*, *AgRP* and *CART* mRNA levels in the Arc were downregulated. *CART*$^{-/-}$ mice displayed elevated adiposity and diminished lean mass across both RT and TN. At RT, *CART*$^{-/-}$ mice showed unchanged food consumption yet greater body weight gain. In addition, an increase in energy expenditure and heightened BAT thermogenesis marked by UCP-1 protein expression was observed in the *CART*$^{-/-}$ mice. In contrast, TN-housed *CART*$^{-/-}$ mice exhibited lower weight gain than WT mice accompanied with pronounced reduction in basal feeding. These findings were correlated with reduced BAT temperature, but unchanged energy expenditure and UCP-1 levels. Interestingly, the respiratory exchange ratio for *CART*$^{-/-}$ mice, which shifted from lower at RT to higher at TN with respect to WT controls, indicates a transition of relative fuel source preference from fat to carbohydrate in the absence of CART signaling. Taken together, these results demonstrate that CART is a critical regulator of energy expenditure, energy partitioning and utilization dependent on the thermal environment.

1. Introduction

Obesity results from the imbalance between energy intake and energy expenditure (Rosen and Spiegelman, 2006). While energy intake is mainly determined by food consumption, energy expenditure comprises basal metabolism for sustenance of the organism, physical activity and various bodily functions like digestion of food, as well as thermogenesis for the maintenance of body temperature through heat dissipation (Hoevenaars et al., 2014; Rosen and Spiegelman, 2006). Current weight-loss approaches mainly target reduction of energy intake, whereas the resultant state of energy deficit is indicated to suppress adaptive thermogenesis and thus decreasing energy expenditure (Major et al., 2007), hampering the effectiveness and sustainability of these treatments. Recently, increasing research interests have focused on the regulation of energy expenditure, which is largely directed by the central nervous system (CNS) at the hypothalamus, particularly through the arcuate nucleus (Arc) (Barsh and Schwartz, 2002; Elmquist et al., 1998; Shi et al., 2013). Within the Arc, two major populations of neurons are well established to modulate energy homeostasis, the orexigenic neuropeptide Y (NPY)/agouti-related protein (AgRP) neurons and the anorexigenic proopiomelanocortin (POMC)/cocaine- and amphetamine-regulated transcript (CART) neurons (Barsh and Schwartz, 2002; Elmquist et al., 1998). In response to peripheral signals reflecting varying nutritional states, such as leptin and peptide YY, the two sets of neurons are differentially regulated to mediate opposing metabolic effects through projections to second-order neurons predominantly located in other hypothalamic regions, namely the paraventricular nucleus (PVN) and lateral hypothalamic area (LHA) (Schwartz et al., 2000). While a wealth of information exists for the roles of NPY, AgRP and POMC, knowledge on CART function remains limited, mainly as the CART receptor(s) are not yet identified.

CART is a key neurotransmitter and hormone involved in the regulation of diverse biological processes, including food intake, maintenance of body weight, reward and addiction, stress response, psychostimulant effects and endocrine functions (Lau and Herzog, 2014; Rogge et al.,

* Corresponding authors at: Neuroscience Division, Garvan Institute of Medical Research, 384 Victoria Street, Darlinghurst, NSW 2010, Sydney, Australia.
E-mail addresses: y.shi@garvan.org.au (Y.-C. Shi), h.herzog@garvan.org.au (H. Herzog).
[1] Equal senior authors.

http://dx.doi.org/10.1016/j.npep.2016.03.006
0143-4179/

2008). CART is strongly conserved between rodents and humans (Dominguez, 2006; Douglass et al., 1995a), and widely expressed in the CNS, with highest levels in the striatal nucleus accumbens (Acb) and various hypothalamic nuclei, including the PVN, LHA, and Arc (Douglass et al., 1995b; Vrang et al., 1999a), suggesting a critical role for CART in appetite control and energy homeostasis. This is supported by findings that *CART* mRNA levels in the PVN and Arc were reduced in response to fasting, while refeeding restored the expression (Kristensen et al., 1998; Vrang et al., 2000). Furthermore, peripheral administration of leptin (Elias et al., 2001; Kristensen et al., 1998) increased *CART* mRNA expression in the Arc, indicating the importance of CART in energy balance regulation. On the other hand, much less is known about a role of CART in controlling energy expenditure. In humans, genetic studies of mutations and polymorphisms in the *CART* gene have shown linkage to alterations in fat distribution (Challis et al., 2000; Rogge et al., 2008) and fat mass, as well as lower metabolic rates and reduced resting energy expenditure which are interrelated with adaptive thermogenesis (Goossens et al., 2009), ultimately corresponding with hyperphagia and elevated body weight that leads to obesity (del Giudice et al., 2001; Guerardel et al., 2005; Kong et al., 2003; Yamada et al., 2002; Yanik et al., 2006). In rats, administration of CART I (55–102) (Dey et al., 2003; Douglass et al., 1995b) intracerebroventricularly (i.c.v.) as well as into the nucleus of the solitary tract in the brainstem has been demonstrated to induce long-lasting hypothermia (Choi et al., 2004; Skibicka et al., 2009). However, the precise role of CART in thermoregulation and the underlying mechanisms are yet to be explored.

In recent years, arguments have arisen to address the influence of housing temperature on the suitability of mouse models in studying human physiology and diseases (Cannon and Nedergaard, 2009; Lodhi and Semenkovich, 2009). In mammals, adaptive thermogenesis is not required when housed in the thermoneutral zone, which is defined as the temperature range within which basal metabolism is sufficient to maintain the core body temperature for adequate physiological and cellular functions (Cannon and Nedergaard, 2011). In contrast, on exposure to colder environments, small mammals and human neonates depend on brown adipose tissue (BAT) action that triggers non-shivering thermogenesis via uncoupling protein-1 (UCP-1) activity for mediating heat dissipation to maintain body temperature (Morrison et al., 2014; Nicholls and Locke, 1984). BAT *UCP*-1 expression in rodents is shown to be modulated by various circulating hormones (Scarpace et al., 1998b) and the i.c.v. administration of specific neuropeptides (Kong et al., 2003; Kristensen et al., 1998; Small et al., 2001). Interestingly, central injection of CART I (55–102) into the PVN or Arc substantially elevated *UCP-1* mRNA expression in BAT, linking CART function beyond feeding control to the modulation of energy expenditure (Kong et al., 2003; Wang et al., 2000). However, concerns have arisen that the operating ambient temperatures of 20–22 °C adopted by mouse facilities are markedly below the proposed thermoneutrality at 28–30 °C (Cannon and Nedergaard, 2009; Karp, 2012), it is therefore questionable whether such thermal range would optimize data translation from mice to humans, who commonly live continuously at thermoneutral temperatures (Cannon and Nedergaard, 2009, 2011; Lodhi and Semenkovich, 2009). The standard housing at 22 °C exposes animals to chronic mild to moderate cold conditioning (Cannon and Nedergaard, 2011; Swoap et al., 2008), where significant allocation of ingested energy to adaptive thermogenesis may introduce confounding factors in the observed phenotypic effects (Ravussin et al., 2012; Speakman and Krol, 2005). In fact, we speculate whether such thermal differences may explain the confounding indications for CART function reported by other studies (Asnicar et al., 2001; Moffett et al., 2006; Wierup et al., 2005). Therefore, thermoneutral housing at 28–30 °C has gained increasing support for maximizing the utility of mouse modeling to mimic human thermal physiology (Cannon and Nedergaard, 2011; Karp, 2012; Lodhi and Semenkovich, 2009).

In this study, we set out to elucidate the regulatory function of CART in energy homeostasis with a focus on the thermoregulatory potential of the peptide using a novel germline *CART* knockout mouse model. Effects of chronic mild cold exposure at 22 °C (RT) were compared with that of the thermoneutral housing at 30 °C (TN), where the energy requirement to maintain normal body temperature is minimized. The metabolic phenotypes along with the underlying mechanisms were examined. In theory, any differential outcomes of CART deficiency between the two thermal conditions will thus support the temperature dependence of CART function and plausibly the overall regulation of energy balance. Therefore, findings from this study may provide consolidation for future work on the therapeutic potential of CART, with modulating energy expenditure as the entry point, in the treatment of obesity and other associated metabolic maladies.

2. Materials and methods

2.1. Animals

All research and animal care procedures were approved by the Garvan Institute/St. Vincent's Hospital Animal Ethics Committee and were in agreement with the Australian Code of Practice for the Care and Use of Animals for Scientific Purposes. Both male and female mice were used for all experiments. All mice were housed under conditions of controlled temperatures of either 22 °C (room temperature, RT) or 30 °C (thermoneutrality, TN) and illumination (12:12 h light–dark cycle, lights on at 07:00 h). Mice were provided with ad libitum access to water and standard chow diet (8% calories from fat, 21% calories from protein, 71% calories from carbohydrate, 2.6 kcal/g; Gordon's Speciality Stock Feeds, Yanderra, NSW, Australia). For the initial pilot study to detect any alteration in *CART* mRNA expression between RT and TN environments, separate cohorts of male C57BL/6J mice fed normal chow were split into two groups; one housed under the normal 22 °C RT condition from birth for 16 weeks (wks), while the other group was transferred to 30 °C TN housing at 9 wks of age for 7 wks. Brains were collected from the 16-wk old mice from both groups and subjected to expression analysis of *CART* mRNA in the hypothalamus.

For the extensive metabolic characterization study, mice were separated into two cohorts. The RT group of *CART* knockout ($CART^{-/-}$) and wild-type (WT) mice was housed under the RT condition from birth for 16 wks until sacrifice. The TN group of $CART^{-/-}$ and WT mice was transferred to housing at the TN zone at 10 wks of age for 10 wks until sacrifice at 20 wks of age; specific experiments were commenced 6 wks after TN exposure. Based on the congruity shown between male and female mice for the majority of the phenotypic traits, together with the greater prominence in phenotypes in males, only data for male mice will be presented.

Fig. 1. Alteration in hypothalamic *CART* mRNA expression at room temperature (RT) versus thermoneutrality (TN) and validation of CART deletion in germline *CART* knockout mice. (A) In situ hybridization of hypothalamic *CART* mRNA expression in male C57BL/6J mice ($n = 6$ per group) from RT (22 °C) and TN (30 °C) conditions. Left: bright-field photomicrographs of coronal brain sections showing *CART* mRNA at the PVN and Arc. Scale bar = 100 μm. Right: hybridization signals are quantified as mean labeling intensity of neurons expressed as percentage coverage of neuronal surface by silver grains (RODs) within the defined areas of interest. Data are means ± SEM and averaged for all mice from each group examined. $^{**}p \leq 0.01$ for WT mice at RT vs. TN. (B) Schematic representation of the *CART-cre* knock-in strategy for generating germline *CART* knockout mouse model, depicting the targeting vector with the floxed neomycin resistance cassette for replacing the *CART* coding exons, the intermediate mutant conditional *CART-cre* knock-in allele, and the homozygous *CART-cre* line representing classical germline *CART* knockout. (C) Representative photomicrographs of the hypothalamus and striatal Acb from WT and $CART^{-/-}$ mice, assessed by in situ hybridization for *CART* mRNA expression. (D) Representative gray-scale photomicrographs display high densities of CART immunostaining within neurons at the Arc and PVN on matching brain sections from WT mice that is absent in $CART^{-/-}$ mice. Scale bars = 100 μm (Arc) and 200 μm (PVN). (E) Representative fluorescence micrographs of brain sections from $CART^{-/-}$ mice displaying the Arc and PVN regions where mCherry red fluorescence protein (RFP) expression within neurons indicates CART deletion. RFP expression was absent in brains from WT mice (data not shown). Insets show higher magnification of the according boxed areas. Scale bar = 100 μm. 3V, third ventricle; PVN, paraventricular nucleus; Arc, arcuate nucleus; Acb, nucleus accumbens.

2.2. Generation of CART knockout mouse model

To investigate the consequences of global *CART* deletion in mice housed at RT against TN, a novel conditional *CART-cre* knock-in mouse line was generated (Fig. 1B). Briefly, the targeting vector was designed to replace the *CART* coding exons with the mouse *Cartpt* cDNA fused to the original *CART* gene at the initiation codon, which is followed by the insertion of a flippase (*Flp*) recombinase-recombination target (*FRT*)-flanked neomycin selection cassette. A cassette carrying the tamoxifen-inducible *Cre*-recombinase gene followed by an internal

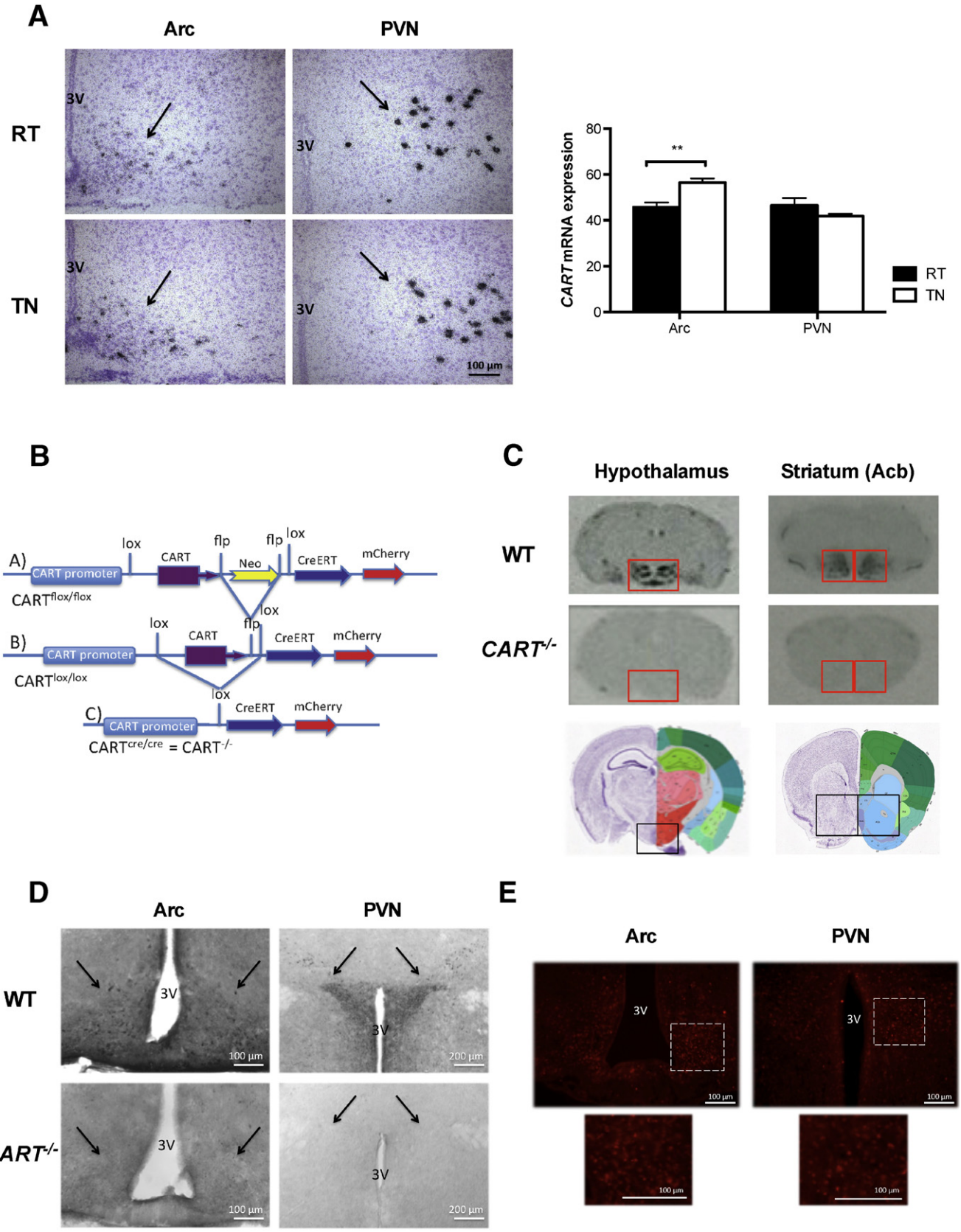

ribosome entry site (IRES) that drives the expression of the mCherry red fluorescence reporter gene was inserted. *LoxP* sites were placed immediately upstream of the initiation codon of the *CART* and *Cre* genes respectively, which allows the replacement of the *CART* gene by *Cre*. Positively targeted ES cell clones were injected into blastocysts. Chimeric offspring were crossed to create heterozygous conditional *CART* mice with the floxed gene ($CART^{lox/+}$), which were then bred with a germline *Flp*-recombinase mouse line to remove the neomycin cassette and further crossed to homozygosity to generate the conditional *CART* floxed knockout line ($CART^{lox/lox}$). The $CART^{lox/lox}$ line was then crossed with mice that expressed *Cre* specifically in the oocytes, resulting in a rearrangement that combines the inducible *Cre* gene with the endogenous *CART* promoter. Subsequent crossing to homozygosity ultimately generated the novel inducible *CART-cre* knock-in mouse line ($CART^{cre/cre}$). Since the endogenous *CART* gene has been replaced by the *Cre*-recombinase gene, the resultant $CART^{cre/cre}$ mice also represent a classical germline *CART* knockout mouse line ($CART^{-/-}$).

2.3. Determination of body weight and food intake

All $CART^{-/-}$ and WT mice housed at 22 °C (RT) and 30 °C (TN) were fed on standard laboratory chow and subject to the same experimental procedures as follows. Body weight was measured weekly throughout the duration of studies. Mice were assessed for spontaneous/basal food intake in the fed state as well as for fasting-induced food intake in response to 24-h fasting at 12 wks (RT) and 16 wks (TN) of age respectively. Basal daily food intake was determined as the average of duplicate readings obtained over two consecutive 24-h periods. Twenty four-h fasting-induced food intake was subsequently measured at 1, 3, 7, and 24 h after refeeding, while the corresponding body weight was recorded in parallel.

2.4. Measurement of whole body and brown adipose tissue temperatures by infrared imaging

Whole body temperature and temperature of the interscapular brown adipose tissue (IBAT) were measured for both the RT (22 °C) and TN (30 °C) cohorts by non-invasive high-sensitivity infrared imaging as described previously (Shi et al., 2013). Briefly, All 12-wk (RT) and 16-wk (TN) old mice were transferred from group housing to individual cages for acclimatization 2 days prior to imaging procedures. For area-specific exposure of skin to facilitate temperature reading, all mice were shaved at the IBAT and lumbar back regions under light isoflurane anesthesia in parallel. A high-sensitivity infrared camera (ThermoCAM T640, FLIR, Danderyd, Sweden, sensitivity = 0.04 °C) fixed on a tripod was placed 100 cm above the freely moving singly housed mouse, and thermographic images were taken for 1 min per mouse. After each 1-min measurement, the camera was moved to record surface temperatures of the next mouse. Temperature measurement was performed daily for three consecutive days under the respective RT or TN condition.

2.5. Indirect calorimetry of energy expenditure and assessment of physical activity

All mice from both the RT (22 °C) and TN (30 °C) groups were evaluated for metabolic parameters and physical activity at 14 and 18 wks of age respectively. For energy metabolism, metabolic rate was measured by indirect calorimetry using an 8-chamber open-circuit calorimeter (Oxymax series; Columbus Instruments, Columbus, OH, USA). Mice were housed individually in specially built Plexiglas cages (20.1 × 10.1 × 12.7 cm). Temperature was maintained at 22 °C or 30 °C according to grouping with airflow of 0.6 L/min. Mice were singly housed for 3 days in home cages prior to acclimatization in Plexiglas cages for 24 h before commencement of recording. Monitoring was subsequently performed for 24 h in the metabolic chambers. Mice were provided with ad libitum access to water and food. Body weight was measured and food given in excess was weighed before and after the recording period for the quantification of daily food intake after subtraction of spillage. Oxygen consumption (VO_2) and carbon dioxide production (VCO_2) were measured every 27 min. The respiratory exchange ratio (RER) was calculated as the quotient of VCO_2/VO_2, with 100% carbohydrate oxidation represented by the value of 1.0 and 100% fat oxidation the value of 0.7. Energy expenditure (kcal heat produced) was determined as calorific value (CV) × VO_2, where CV is 3.815 + 1.232 × RER. Data obtained for the 24-h monitoring period were averaged at 1-h intervals for energy expenditure and RER.

For physical activity, ambulatory activity of the mice was assessed in parallel within the Plexiglas metabolic chambers with an OPTO-M3 sensor system (Columbus Instruments, Columbus, OH, USA). Ambulatory counts denote the consecutive adjacent photo-beam breaks, while cumulative ambulatory counts of the X, Y and Z directions were recorded per minute and summed at 1-h intervals.

2.6. Body composition and bone densitometry analysis

All mice from both RT (22 °C) and TN (30 °C) groups were subjected to an initial body composition analysis using the dual-energy X-ray absorptiometry (DXA) (Lunar PIXImus2 mouse densitometer; GE Healthcare, Waukesha, WI, USA) system at 10 and 14 wks of age respectively. A second DXA scan was performed 4 wks after initial DXA measurements. Animals were anesthetized with isoflurane for the scanning procedure to determine whole body bone mineral density (BMD), bone mineral content (BMC), fat and lean mass, where lean mass corresponds to non-fat and non-bone tissue content. The head of the animal was excluded while the tail included for the analysis.

2.7. Tissue collection

Following completion of studies, all mice from both RT (22 °C) and TN (30 °C) groups were sacrificed at 16 and 20 wks of age respectively. Animals were culled between 1300 and 1700 h through cervical dislocation followed by decapitation. Brains were promptly collected and frozen on dry ice, then stored at −80 °C until subsequent analysis as described below. The brown adipose tissue (BAT) at the interscapular area and the white adipose tissue (WAT) depots from the inguinal, epididymal or periovarian (gonadal), retroperitoneal and mesenteric regions were removed and weighed. Tissue weights are normalized and expressed as a percentage of body weight.

2.8. In situ hybridization analysis of mRNA expression of key hypothalamic neuropeptides

In situ hybridization was performed on brain sections of WT ($n \geq 5$) and $CART^{-/-}$ ($n \geq 5$) mice from both RT (22 °C) and TN (30 °C) groups to determine mRNA expression of tyrosine hydroxylase (*TH*), corticotropin-releasing hormone (*CRH*), thyrotropin-releasing hormone (*TRH*), *CART*, *NPY*, *AgRP* and *POMC* at the hypothalamus following procedures as previously described (Sainsbury et al., 2002; Shi et al., 2013). Briefly, matching coronal brain sections (25 μm) collected from the WT and $CART^{-/-}$ mice were prepared from specific brain levels with respect to the bregma to represent the hypothalamic PVN for the detection of *TH*, *CRH*, and *TRH* mRNA, the striatal Acb and the hypothalamic PVN and Arc for detection of *CART* mRNA, and the Arc for *NPY*, *AgRP* and *POMC* mRNA detection. The cryosections were hybridized with [α-^{35}S]-thio-dATP (PerkinElmer, Boston, MA, USA) radiolabeled DNA oligonucleotides complementary to mouse *TH* (5′-CTCTAAGGAG CGCCGGATGGTGTGAGGACTGTCCAGTACATCA-3′), *CRH* (5′-CCGATAAT CTCCATCAGTTTCCTGTTGCTGTGAGCTTGCTGAGCT-3′), *TRH* (5′-AACCTT ACTCCTCCAGAGGTTCCCTGACCCAGGCTTCCAGTTGTG-3′), *CART* (5′-TCCTTCTCGTGGGACGCATCATCCACGGCAGAGTA GATGTCCAGG-3′), *NPY* (5′-GAGGGTCAGTCCACACAGCCCCATTCGCTTG TTACCTAGCAT-3′),

ArRP (5′-AGCTTGCGGCAGTAGCAAAAGGCATTGAAG AAGCGGCAGTAG CAC-3′) and *POMC* (5′-TGGCTGCTCTCCAGGCACCAGC TCCACACATCTA TGGA-GG-3′). Hybridization signals on sections were visualized by exposure to BioMax MR film (Kodak, Rochester, NY, USA) for 7–10 days and digitalized images from the scanned autoradiograms were acquired. For structural details, the brain sections were photoemulsion-dipped and superficially counterstained with hematoxylin, with which regions of interest were visualized and captured into digital images acquired by bright-field microscopy. Quantification of the mRNA expression levels of respective genes was performed by measuring the relative optical densities (RODs) within the brain areas of interest outlined with consistent defined dimensions across corresponding sections on the photomicrographs using the National Institutes of Health ImageJ 1.61 software (written by Wayne Rasband; available from anonymous FTP at zippy.nimh.nih.gov). Background labeling was considered uniform with signal levels below 5% of specific signal levels and was subtracted from the resultant signal density. Data are evaluated and presented as percentage of ROD averaged from at least three sections per mRNA assessed per animal.

2.9. Western blot analysis of protein expression in BAT

Western blot analysis was performed on BAT samples of WT ($n \geq 3$) and *CART*$^{-/-}$ ($n \geq 3$) mice from RT (22 °C) and TN (30 °C) groups to determine the protein expression of UCP-1, peroxisome proliferator-activated receptor (PPAR)-γ coactivator (PGC)-1α, carnitine palmitoyltransferase-1 (CPT-1) and glyceraldehyde 3-phosphate dehydrogenase (GAPDH) following procedures previously described (Shi et al., 2010). In brief, BAT samples were homogenized in RIPA buffer (25 mM Tris–HCl pH 7.6, 150 mM NaCl, 1% NP-40, 1% sodium deoxycholate and 0.1% SDS) supplemented with protease inhibitor cocktail tablets (cOmplete™ Mini, Roche Diagnostic, Mannheim, Germany) and subsequent centrifugation. Clear lysates were collected for determination of total protein concentration on a spectrophotometer (Spectramax® Plus 384 Microplate Reader, Molecular Devices, Silicon Valley, CA, USA) using the Bradford dye-binding method. Equal amounts of tissue lysate (20 μg protein) were resolved by SDS-polyacrylamide gel electrophoresis and immunoblotted with antibodies against UCP-1 (Alpha Diagnostic, San Antonio, TX, USA), PGC-1α (Calbiochem, Merck Pty. Ltd., Kilsyth, VIC, Australia), CPT-1 (Santa Cruz Biotechnology, Santa Cruz, CA, USA) and GAPDH (Cell Signaling Technology, Genesearch Pty. Ltd., Arundel, Australia). Immunolabeled bands were quantified by densitometry. Relative expression for the proteins of interest was normalized to the expression level of the housekeeper GAPDH.

2.10. Confirmation of CART ablation in *CART*$^{-/-}$ mice

Germline *CART* deletion in *CART* knockout mice was verified through the following techniques (Fig. S1). At the DNA level, genomic DNA from WT and *CART*$^{-/-}$ mice was isolated from the fresh frozen livers and subjected to polymerase chain reaction (PCR) assessment for genotype. PCR was performed using the primer sets: CART-F (5′-GCTGCCTACA GACGGCTGAC-3′) with Cre-A (5′-ACATCTTCAGGTTCTGCG-3′), CART-F with CART-R (5′-GGAGCTCTCCATGGTTCTGG-3′), and Cre-F (5′-CTGG TGTAGCTGATGATCC-3′) with Cre-R (5′-TTTCACTATCCAGGTTACGG-3′). PCR with CART-F/Cre-A was designed to produce 430 bp fragments representing deletion of the entire *CART* gene cluster flanked by recombinase recognition loxP sites (floxed) to be expected in *CART*$^{-/-}$ samples. The genotypes were further examined with PCR primed by CART-F/CART-R oligos for the generation of 172 bp amplicons representing part of the *CART* gene sequence to be expected in WT samples. Replacement of the endogenous *CART* gene by *Cre* in *CART*$^{-/-}$ (*CART*$^{cre/cre}$) mice was also investigated using Cre-F/Cre-R primer pair for the production of ~300 bp amplicons.

At the transcriptional level, in addition to validation of *CART* mRNA ablation by in situ hybridization on brain cryosections from WT ($n = 7$) and *CART*$^{-/-}$ ($n = 11$) mice as described above, deletion efficiency was determined through examining central *Cre* and *mCherry* mRNA expression levels in the hypothalamus from WT ($n \geq 3$) and *CART*$^{-/-}$ ($n \geq 3$) mice. Total RNA from the dissected hypothalamus was extracted using TRIzol® reagent (Sigma, St Louis, MO, USA) following manufacturer's protocol. The purity and concentration of RNA was assessed using a spectrophotometer (Nanodrop® ND-1000 UV–Vis Spectrophotometer; Nanodrop Technologies, DE, USA). Total RNA of 1 μg from each subject was reverse transcribed into cDNA using the SuperScriptTM III First-Strand cDNA Synthesis System for RT-PCR (Invitrogen, Mount Waverley, VIC, Australia) according to manufacturer's instructions. PCR was subsequently conducted on a Veriti® thermal cycler (Applied Biosystems, Foster City, CA, USA) with the cDNA samples primed by the oligo pairs Cre-F (5′-CTGGTGTAGC TGATGATCC-3′) with Cre-R (5′-TTTCACTATCCAGGTTACGG-3′) and mCherry-F (5′-GAGTTCATGCGCTTCAAGGT-3′) with mCherry-R (5′-TGGGAGGTGATGTCCAACTT-3′) for the evaluation of *Cre* and *mCherry* mRNA expression respectively.

At the translational level, ablation of CART peptide was determined by examining the protein expression of CART and mCherry through immunohistochemistry as previously described (Shi et al., 2013), and direct fluorescence microscopy respectively. For both experiments, WT and *CART*$^{-/-}$ mice were anesthetized with intraperitoneal injection of 100/20 mg/kg ketamine/xylazine (Parke Davis-Pfizer, Sydney, Australia & Bayer AG, Leverkusen, Germany) and the brains were subsequently fixed by perfusion with 0.9% saline followed by ice-cold 4% paraformaldehyde (PFA) in 0.1 M phosphate buffered saline (PBS) (pH 7.4). Brains were promptly collected and post-fixed in 4% PFA for 6 h prior to cryoprotection in 30% sucrose solution overnight. Coronal brain slices (30 μm) were cryosectioned and stored in 0.1% PBS-Triton X-100 (PBST). For the detection of CART peptide by immunohistochemistry, cryosections from WT ($n = 5$) and *CART*$^{-/-}$ ($n = 6$) mice were immunostained overnight with rabbit anti-mouse CART polyclonal primary antibody Ca7-OVA (Vrang et al., 1999b) (gift from Dr. Anna Secher, Novo Nordisk, Copenhagen, Denmark) diluted 1:1500 in PBST, followed by incubation with biotinylated goat anti-rabbit IgG secondary antibody (Vector Laboratories, Burlingame, CA, USA) diluted 1:250 for 2 h. Sections were then incubated with ExtrAvidin-peroxidase (Sigma-Aldrich, St. Louis, MO, USA) and immunostained for CART expression using diaminobenzidine (Dako, Carpinteria, CA, USA) as the chromogen. Free-floating brain sections were mounted on Superfrost® slides and coverslipped. For visualization of CART immunoreactivity, hypothalamic regions rich in endogenous CART expression were investigated in WT and *CART*$^{-/-}$ brain sections by bright-field microscopy. Photomicrograph were acquired for brain regions containing neurons with CART expression present in WT while absent in *CART*$^{-/-}$ samples.

In separate experiments, free-floating brain sections from WT and *CART*$^{-/-}$ ($n = 3$ each) mice were prepared as described above and mounted on Superfrost® slides for the detection of mCherry expression by direct fluorescence microscopy. To detect red fluorescence protein (RFP) expression produced by the *mCherry* reporter coupled to the targeting construct, hypothalamic regions with rich endogenous CART expression were examined in WT and *CART*$^{-/-}$ brain sections using a Zeiss Axiophot microscope equipped with a ProgRes 3008 digital camera (Carl Zeiss, Jena, Germany). Fluorescence micrographs were acquired for the visualization of RFP expression indicative of CART deletion in *CART*$^{-/-}$ brains in regions otherwise containing CART-positive neurons in the corresponding RFP-negative WT counterparts.

2.11. Statistical analysis

All data are presented as means ± SEM. Differences amongst mouse groups of various genotypes and thermal conditions were assessed by ANOVA or repeated-measures ANOVA combined with Bonferroni

post-hoc analysis where appropriate. Energy expenditure, RER and physical activity over the continuous 24-h period were averaged for the whole 24-h period, as well as the 12-h light and dark phases individually. Comparison of energy expenditure (kcal/h) between groups was performed by the analysis of covariance (ANCOVA) with lean mass as the covariate. The adjusted means of energy expenditure at a common lean mass for the comparison were generated by ANCOVA as presented. Statistical analyses were performed with GraphPad Prism 6 for Mac OS X (GraphPad Software, Inc. CA, USA) and SPSS for Mac OS X version 16.0.1 (SPSS Inc., Chicago, IL, USA). Statistical significance was defined as p-value ≤0.05.

3. Results

Hypothalamic CART has been linked to the modulation of energy expenditure and thermoregulation in mice (Choi et al., 2004; Kong et al., 2003; Skibicka et al., 2009; Wang et al., 2000); however, the majority of these studies are performed at 22 °C, a temperature which is considered a mild chronic cold exposure that can alter overall energy homeostasis. To determine whether exposure of mice to 22 °C temperature condition (RT) against 30 °C thermoneutral condition (TN) could influence *CART* expression, analysis of hypothalamic *CART* mRNA levels was performed on brains collected from male C57BL/6JAusb mice housed under the two thermal conditions (Fig. 1A). As the hypothalamic Arc and PVN both contain abundant *CART* expression and represent areas of interest for a thermoregulatory role of CART, in situ hybridization was performed on representative brain sections matched between RT and TN groups. While no significant difference in *CART* mRNA levels was detected in the PVN between RT and TN conditions, the TN-housed mice showed significantly upregulated *CART* expression in the Arc compared to the RT group (Fig. 1A). This suggests a potential role for Arc CART in thermoregulation, which could subsequently impact energy homeostasis. To further explore this hypothesis, a novel germline *CART* knockout mouse model was generated to study the specific role of CART in energy homeostasis regulation under RT and TN conditions.

3.1. Successful generation of a novel CART knockout mouse model

The targeting strategy for generating the novel conditional *CART-cre* knock-in mouse line is illustrated in Fig. 1B, with the detailed procedures described in the Materials and methods section. Validation of global *CART* ablation in the germline *CART* knockout mouse model was attained via direct and indirect evaluations of CART expression on the DNA sequence, transcriptional and translational levels. Successful deletion of the *CART* coding sequence was confirmed on the genomic DNA by a combination of different PCR strategies that either produced or no longer produced amplicons after CART deletion (Fig. S1). The presence of *Cre*-recombinase and *mCherry* transgene expression was also confirmed on the mRNA level by RT-PCR in *CART* knockout mice in which the deletion had occurred (Fig. S1). Successful ablation of *CART* mRNA expression was confirmed by in situ hybridization in the hypothalamus and striatum (Fig. 1C), the brain regions rich in endogenous *CART* expression (Douglass et al., 1995b; Vrang, 2006). Immunohistochemistry further confirmed the absence of CART protein expression at the Arc and PVN (Fig. 1D) in $CART^{-/-}$ mice compared to WT mice. Finally, expression of mCherry reporter fluorescence indicated loss of the *CART* gene in the Arc and PVN of $CART^{-/-}$ mice (Fig. 1E) compared to WT brain (data not shown).

3.2. Differential effects of CART deletion on weight gain at different temperatures

$CART^{-/-}$ mice were born in the expected Mendelian ratio; no significant differences in appearance or body weight were observed at birth between these mice and their control littermates (data not shown). In order to investigate the baseline metabolic characteristics of this novel $CART^{-/-}$ model under RT and TN conditions, we first measured body weight (BW) and food intake under standard chow diet and RT conditions. Data from this group were then compared with phenotypic measurements from a separate cohort of $CART^{-/-}$ and WT mice housed at TN conditions.

$CART^{-/-}$ animals gained similar body weight to control mice when expressed in absolute weight at either thermal condition (Fig. 2A). There was no notable temperature-related difference in absolute body weight between mice from RT and TN groups. However, $CART^{-/-}$ mice showed significantly increased body weight gain when expressed as a percentage of initial body weight at RT (Fig. 2B). Conversely, TN-housed $CART^{-/-}$ mice exhibited a significant decrease in percentage body weight gain over time compared with WT controls (Fig. 2B). In addition, TN-housed $CART^{-/-}$ and WT mice exhibited less body weight gain in general compared with mice at RT (Fig. 2B).

3.3. CART ablation promotes adiposity accretion and reduces lean mass

To elucidate the factors contributing to the differential body weight gain across thermal environments, body composition analysis was performed. DXA analysis revealed a substantially higher whole body fat mass expressed as a percentage of BW in $CART^{-/-}$ mice relative to WTs at both housing temperatures (Fig. 2C), with a more pronounced increase in $CART^{-/-}$ mice in the TN group. Fat mass did not differ between the same genotype under RT and TN conditions. The elevated fat mass in $CART^{-/-}$ mice from both RT and TN was also confirmed by increased mass of dissected white adipose tissue (WAT) depots (expressed as a percentage of BW) in $CART^{-/-}$ mice (Fig. 2D). In contrast to the increase in fat mass, whole body lean mass presented as a percentage of BW showed a trend to a reduction in $CART^{-/-}$ mice at RT compared with WT, with a significant reduction in $CART^{-/-}$ mice at TN condition (Fig. 2E). Again, no difference in lean mass was detected in mice of the same genotypes between temperatures.

3.4. Thermoneutrality rescues the bone mass reduction in CART knockout mice

As CART is also considered one of the neuropeptides linking energy homeostasis and bone remodeling (Elefteriou et al., 2005; Gerrits et al., 2011), DXA scans for bone mineral density and content were performed (Fig. 2F, G). Significant reduction in both whole body BMD (Fig. 2F) and BMC (Fig. 2G) was shown in $CART^{-/-}$ mice at RT compared to WT controls, further supporting a role of CART in modulating bone modeling. Interestingly, such genotype difference was absent in TN-housed animals, suggesting a critical function of CART to provide protection from bone loss under moderate cold conditioning such as exposure to 22 °C at RT.

3.5. Differential effects of CART deletion on food intake at different temperatures

To explore the effects of CART ablation on appetite regulation under RT and TN conditions, spontaneous/basal and fasting-induced food

Fig. 2. *CART* deletion reduced weight gain and basal food intake at thermoneutrality despite increased adiposity at both thermal conditions. (A) Absolute body weight (BW) measured weekly in WT (n = 9–12) and $CART^{-/-}$ (n = 9–12) mice at both room temperature (RT) and thermoneutrality (TN). (B) Corresponding BW change in proportion to initial body BW. Whole body (C) fat mass and (E) lean mass as a percentage of body weight (%BW) as determined by body composition analysis using dual-energy X-ray absorptiometry (DXA). (D) Tissue mass (%BW) of dissected white adipose tissue (WAT) depots after sacrifice of mice. i, inguinal; e, epididymal; m, mesenteric; r, retroperitoneal; total, summed weight of i, e, m and r WAT depots. Whole body (F) bone mineral density (BMD) and (G) bone mineral content (BMC) determined by DXA. Spontaneous/basal (H) and accumulative 24-h fasting-induced (I) food intake (%BW). Data are means ± SEM and averaged for all mice from each group examined. $^{*}p \le 0.05$, $^{**}p \le 0.01$, $^{***}p \le 0.001$, $^{****}p \le 0.0001$ for $CART^{-/-}$ versus WT mice, for comparisons between the same genotype across thermal conditions, or for comparisons indicated by horizontal bar.

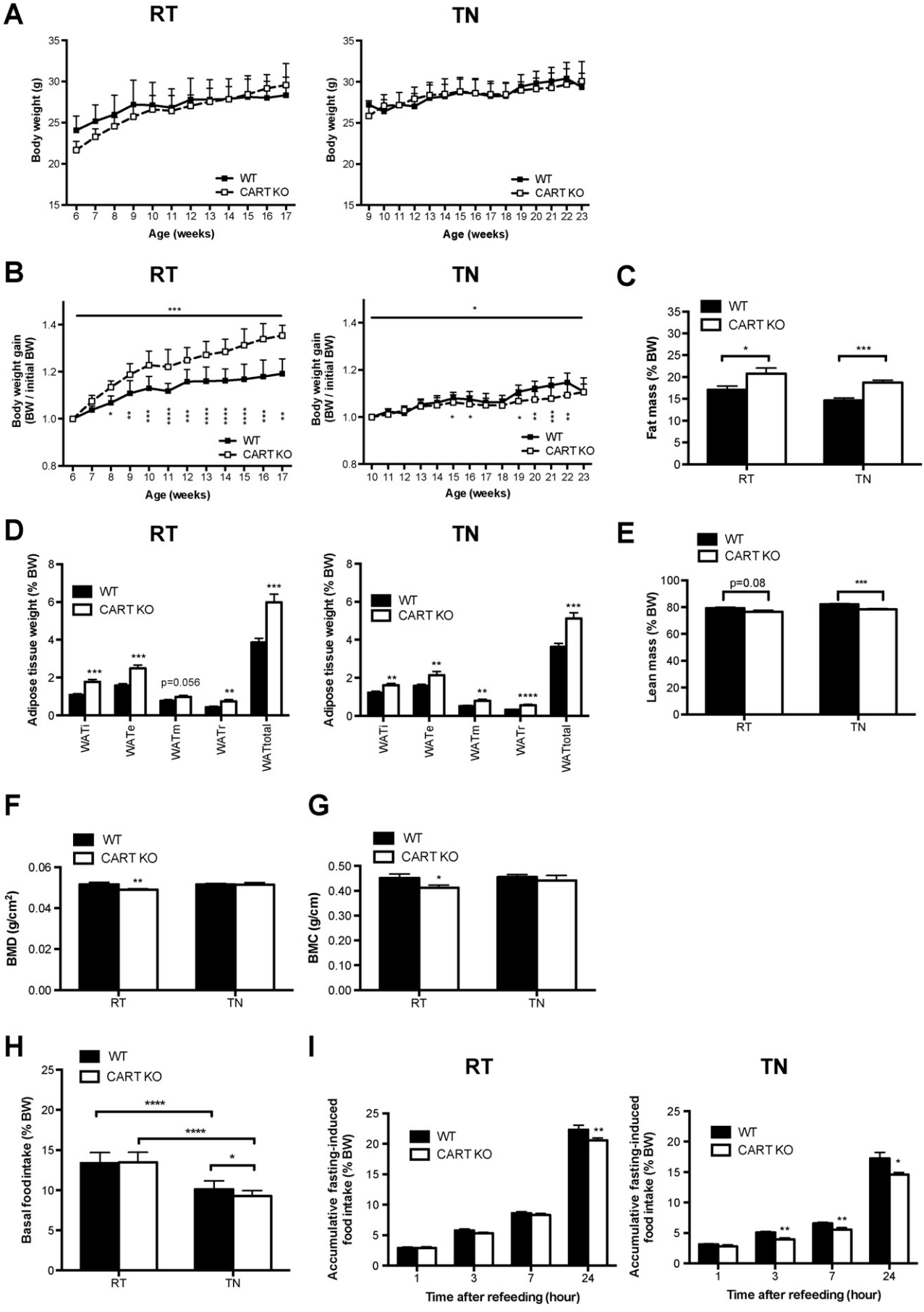
A
RT
TN
Body weight (g)
Age (weeks)
WT
CART KO
B
RT
TN
Body weight gain (BW / initial BW)
Age (weeks)
C
Fat mass (% BW)
RT
TN
D
RT
TN
Adipose tissue weight (% BW)
WATi
WATe
WATm
WATr
WATtotal
p=0.056
E
Lean mass (% BW)
p=0.08
F
BMD (g/cm²)
G
BMC (g/cm)
H
Basal food intake (% BW)
I
RT
TN
Accumulative fasting-induced food intake (% BW)
Time after refeeding (hour)

intake were measured in *CART*$^{-/-}$ and WT mice. Twenty four-hour basal food intake (expressed as a percentage of BW) was unaltered between RT-housed *CART*$^{-/-}$ and WT groups (Fig. 2H), therefore unlikely to be a contributing factor to the marked increase in body weight gain seen in *CART*$^{-/-}$ mice. Interestingly, thermoneutrality significantly reduced food intake in both *CART*$^{-/-}$ and WT mice, even though mice housed at RT and TN demonstrated comparable absolute body weight. Further to such downregulation in baseline feeding at TN, *CART*$^{-/-}$ mice housed at TN exhibited notably stronger reduction in spontaneous food intake compared with WT controls (Fig. 2H), consistent with the significant decline in body weight gain. Daily fecal output in *CART*$^{-/-}$ mice was not different between the two groups under both thermal conditions (data not shown), eliminating potential effects of nutrient resorption in the gut as a cause for the observed phenotype. Food intake in response to 24-h fasting (expressed as a percentage of BW) in *CART*$^{-/-}$ mice was reduced compared to WT controls at RT, and the difference reached statistical significance at 24 h after refeeding (Fig. 2I). Similar to spontaneous food intake, fasting-induced feeding under thermoneutral condition was generally reduced for both WT and *CART*$^{-/-}$ mice. Again, the effects of TN on downregulating feeding were more pronounced in *CART*$^{-/-}$ compared to WT mice, with a statistically significant reduction shown as early as 3 h following refeeding (Fig. 2I). *CART*$^{-/-}$ mice at both thermal conditions showed similar body weight recovery compared with WT counterparts after 24-h fasting (Fig. S2).

3.6. CART deficiency promotes energy expenditure while reducing RER in mice

In light of the differential phenotypes exhibited in food consumption and weight gain between genotypes and thermal conditions, along with the altered lean body mass, which is a major determinant of heat dissipation, open-circuit indirect calorimetry was applied to elucidate the metabolic modulations potentially associated with CART deficiency under the two housing temperatures. *CART*$^{-/-}$ and WT controls at RT and TN were evaluated for parameters of energy expenditure, respiratory quotient and physical activity under free-feeding conditions. A marked increase in energy expenditure was demonstrated in *CART*$^{-/-}$ relative to WT mice at RT (Fig. 3A), both overall and specifically during the light phase, which could be a compensatory response to the observed increase in body weight gain (Fig. 2B). However, such an increase was absent in TN-housed *CART*$^{-/-}$ compared with WT controls (Fig. 3A). Evaluation of non-genotype-specific alterations between RT and TN groups identified a prominent increase in average energy expenditure in both WT and *CART*$^{-/-}$ mice housed at RT relative to TN over the total 24-h period (Fig. 3B). Interestingly, the elevated energy expenditure observed in RT-housed *CART*$^{-/-}$ mice was not associated with any corresponding increase in physical activity (Fig. 3C), indicating physical activity did not contribute to increased energy expenditure under this thermal condition. Consistent with unaltered energy expenditure at TN, no detectable differences were observed in physical activity between genotypes (Fig. 3C). Furthermore, the significantly higher energy expenditure in RT-housed mice (Fig. 3B) was associated with a corresponding marked increase in overall physical activity when compared with TN counterparts regardless of genotype (Fig. 3D).

RER, an index of metabolic fuel selection, in *CART*$^{-/-}$ mice was significantly lower than that of WT mice at RT (Fig. 3E), notably so in the dark phase, suggesting an increased relative preference for fat over carbohydrate as the metabolized fuel in RT-housed *CART* knockouts. In contrast, TN-housed *CART*$^{-/-}$ mice displayed a strong trend towards elevated RER compared to WT counterparts, particularly during the dark phase ($p = 0.12$, Fig. 3E, F), further indicating a differential role of CART signaling in regulating oxidative fuel selection under different environmental temperatures (Fig. 3E, F). Moreover, TN-housed WT mice showed a pronounced decrease in RER over the 24-h period compared with RT counterparts (Fig. 3F), indicating an enhanced fuel source preference for fat over carbohydrate under thermoneutral condition. This decrease was not observed in *CART*$^{-/-}$ mice.

3.7. CART deficiency promotes BAT UCP-1 expression in mice

Since BAT activity is responsible for non-shivering thermogenesis via UCP-1 activation, we next examined the contribution of BAT to overall metabolism. Interestingly, BAT weight (expressed as a percentage of BW) was substantially increased in *CART*$^{-/-}$ mice relative to WT at both TN and RT, and the difference became statistically significant at TN (Fig. 3G). While WT mice at TN showed a nominal decrease in BAT weight relative to RT, *CART*$^{-/-}$ mice exhibited significantly lower BAT weight at TN compared to RT (Fig. 3G). Consistent with the higher BAT weight in *CART*$^{-/-}$ mice, expression levels of UCP-1 were moderately elevated in RT-housed *CART*$^{-/-}$ compared to WT mice (Fig. 3H). Such an increase was absent in TN-housed counterparts. It is noteworthy that the baseline levels of UCP-1 were significantly downregulated in TN mice compared to the RT cohort for both genotypes, especially distinctive for *CART*$^{-/-}$ mice (Fig. 3H). In addition, protein expression levels of PGC-1α, a critical transcriptional regulator of mitochondrial oxidative metabolism and UCP-1 expression (Puigserver et al., 1998), showed no significant difference between genotypes or across thermal conditions (Fig. 3H). Nevertheless, a trend of reduction in PGC-1α expression was notable in *CART*$^{-/-}$ compared to WT mice at both RT and TN. A similar expression pattern was indicated for CPT-1, a key mitochondrial transmembrane enzyme catalyzing the entry of long-chain fatty acid for oxidation in a rate-limiting manner (Bonnefont et al., 2004). Significant differences between genotypes or temperatures were not detected in CPT-1 protein expression, which however, showed a trend to downregulation in *CART*$^{-/-}$ with respect to WT mice at both RT and TN (Fig. 3H). In contrast with the increased energy expenditure in *CART*$^{-/-}$ mice compared to WT at RT, no alteration in body temperature was identified between genotypes (data not shown). On the contrary, despite unchanged energy expenditure in *CART*$^{-/-}$ mice at TN, infrared imaging detected a pronounced reduction in BAT temperature compared with WT, whereas whole body temperature represented by measurements of the lumbar back control area was unaltered (Fig. 4A).

3.8. Alterations in hypothalamic expression of several key peptides in the control of energy homeostasis

In order to determine the central mechanisms underlying the *CART* knockout phenotypes manifested under the two thermal conditions, hypothalamic expression of various neurotransmitters and hormones that are important in the regulation of adaptive thermogenesis and energy homeostasis were profiled. In situ hybridization was performed to examine the transcript expression of *TH* and *CRH* in the PVN, as the expression levels of both in the PVN have been linked to the modulation of energy expenditure and BAT thermogenesis (Richard et al., 2002; Shi et al., 2013). Importantly, a significant reduction in the PVN mRNA levels of *TH*, a rate-limiting enzyme in the synthesis of catecholamines (Zhou et al., 1995), was observed in *CART*$^{-/-}$ compared to WT mice at RT only (Fig. 4B). Similarly, a modest decrease in *CRH* mRNA expression in the PVN was shown in *CART*$^{-/-}$ compared to WT mice at RT, while no genotype difference was detected in the TN groups (Fig. 4C). With regard to temperature effects, baseline *TH* and *CRH* expression were markedly downregulated in mice of both genotypes at TN compared to RT conditions. In addition to CRH (Richard et al., 2002), TRH represents another pivotal regulator of the hypothalamic–pituitary–adrenal axis with implicated roles in the control of energy balance and thermoregulation (Joseph-Bravo, 2004), where TRH-synthesizing neurons are largely populated in the PVN (Lechan and Fekete, 2006). In contrast to the above, the expression level of *TRH* mRNA in the PVN lacked genotypic differences regardless of thermal conditions; however, baseline *TRH* levels in both genotypes were reduced under TN conditions (Fig. 4D).

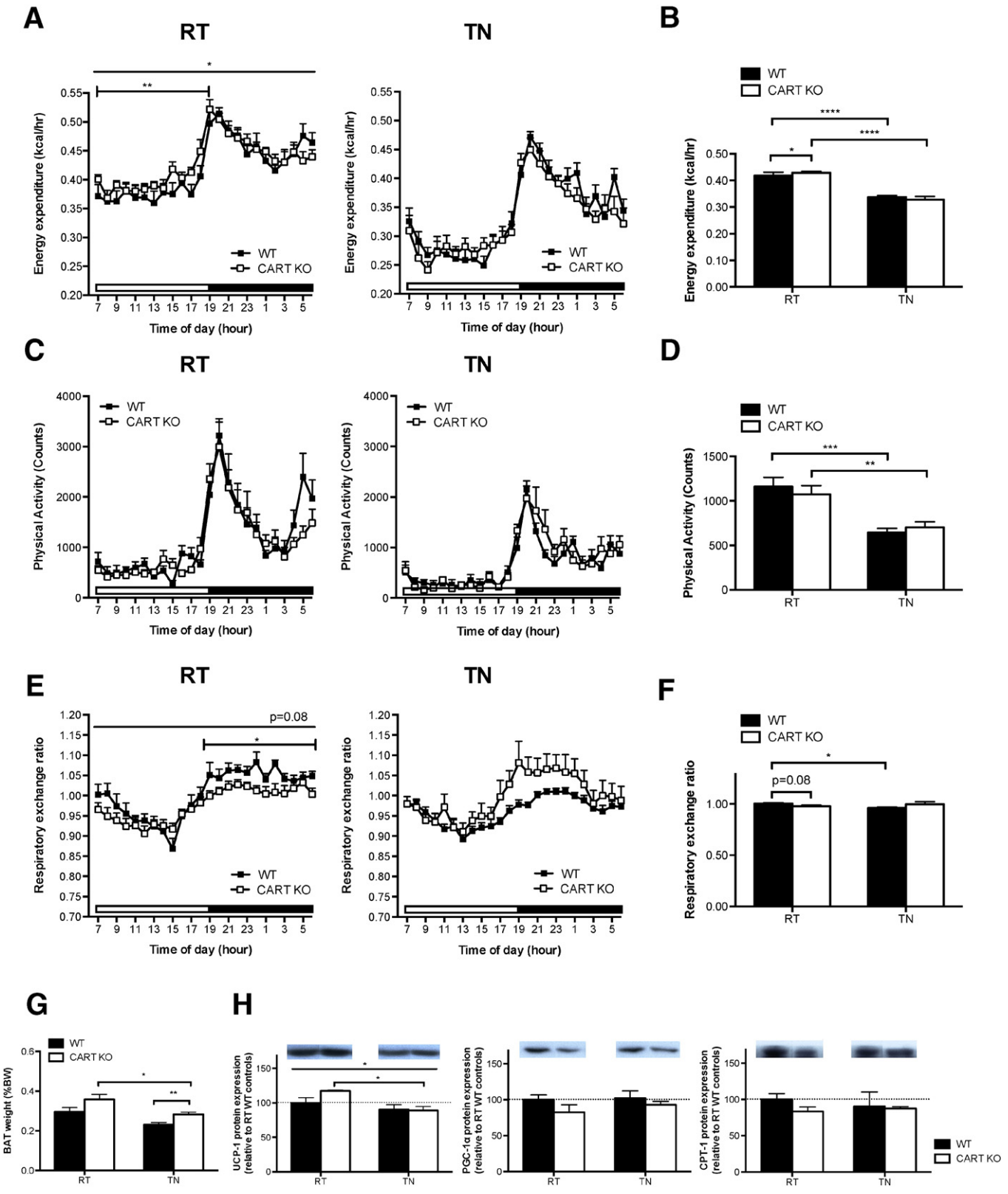

Fig. 3. Absence of CART stimulates energy expenditure and BAT activity while lowers respiratory exchange ratio at room temperature (22 °C). Indirect calorimetric assessments for the 24-h time course of energy expenditure (A, B), physical activity (C, D) and respiratory exchange ratio (E, F) in WT and *CART*$^{-/-}$ mice housed at room temperature (RT) and thermoneutral (TN) conditions. Corresponding average values for each parameter over the total 24-h period were shown in adjacent bar graphs. Energy expenditure was adjusted for lean mass and compared between groups by analysis of covariance. The adjusted means of energy expenditure were presented at the common lean mass of 21.381 g (RT) and 22.9 g (TN) respectively. Open and filled horizontal bars indicate the light and dark photoperiods, respectively. (G) Dissected brown adipose tissue (BAT) mass as a percentage of body weight. (H) Western blot quantification of UCP-1, PGC-1α and CPT-1 protein expression in the BAT of WT and *CART*$^{-/-}$ mice from RT and TN, with GAPDH as loading control. Images are representative of at least three mice per group. Data are means ± SEM and averaged for all mice from each group examined. $^{*}p \le 0.05$, $^{**}p \le 0.01$, $^{***}p \le 0.001$, $^{****}p \le 0.0001$ for *CART*$^{-/-}$ versus WT mice or for comparisons between the same genotype across thermal conditions.

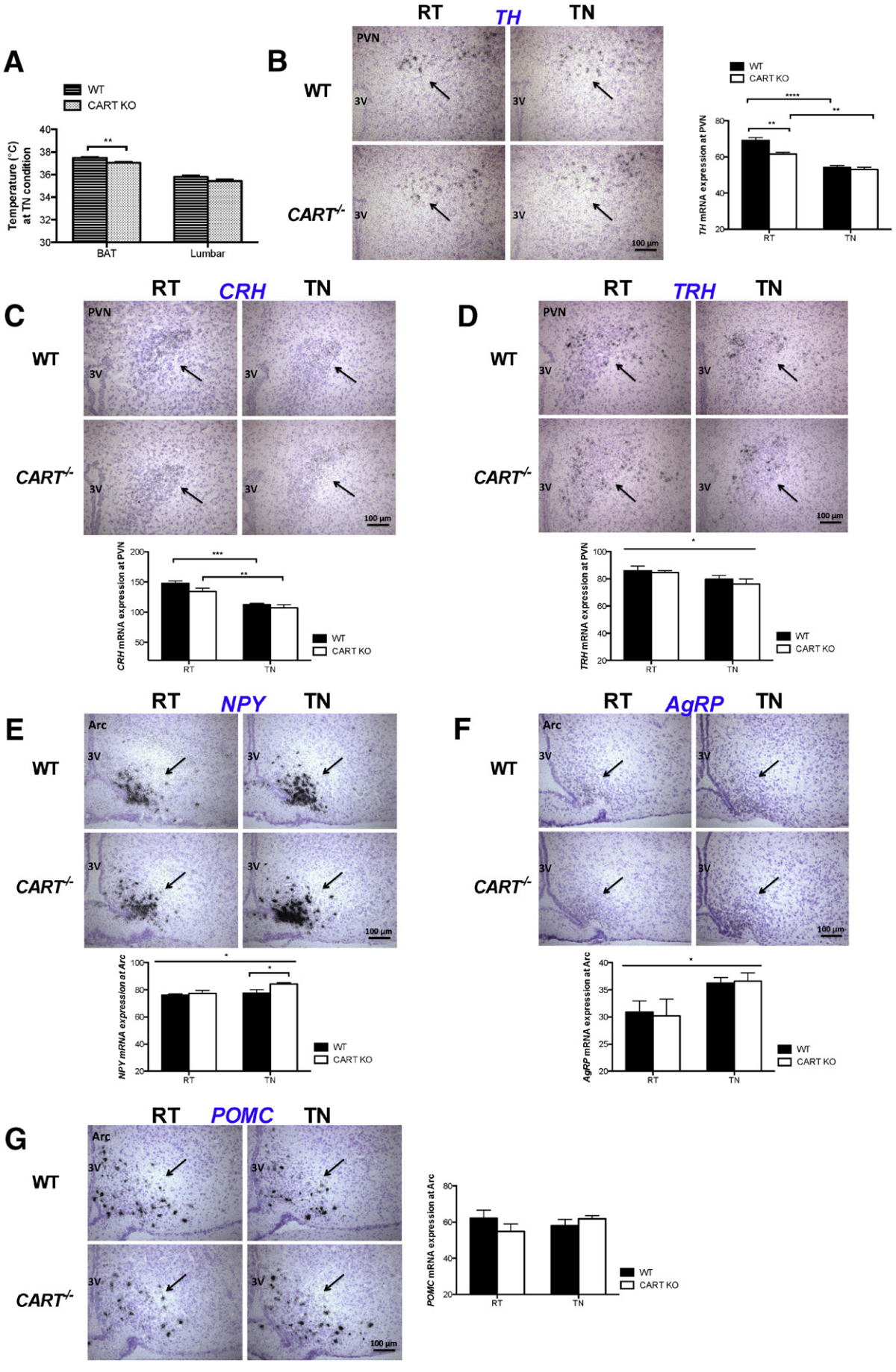
A
WT
CART KO
Temperature (°C) at TN condition
BAT
Lumbar
B
RT
TH
TN
PVN
3V
WT
CART-/-
100 μm
TH mRNA expression at PVN
C
CRH
PVN
CRH mRNA expression at PVN
D
TRH
TRH mRNA expression at PVN
E
NPY
Arc
NPY mRNA expression at Arc
F
AgRP
AgRP mRNA expression at Arc
G
POMC
POMC mRNA expression at Arc

In addition to the above factors, expression levels of major neuropeptides in the hypothalamic Arc that are critical in feeding control and also exhibiting thermogenic properties were assessed by in situ hybridization. Although unchanged between genotypes at RT, Arc *NPY* mRNA levels were significantly increased in *CART*$^{-/-}$ compared to WT mice at TN (Fig. 4E). Prominent temperature effects were also evident in the significantly higher baseline *NPY* expression in both *CART*$^{-/-}$ and WT mice at TN compared to RT conditions (Fig. 4E). Similarly, *AgRP* mRNA levels in the Arc were markedly upregulated in TN-housed mice of both genotypes compared with RT counterparts, despite unaltered expression levels between *CART*$^{-/-}$ and WT mice (Fig. 4F). On the contrary, temperature effects were undetected in Arc *POMC* levels in mice between RT and TN housing, while significant difference was also absent between *CART*$^{-/-}$ and WT mice regardless of thermal conditions (Fig. 4G).

4. Discussion

In the present study, we demonstrate for the first time the differential roles of CART signaling in the regulation of energy homeostasis under different housing temperatures: room temperature at 22 °C and thermoneutrality at 30 °C. Housing *CART* knockout mice at room temperature resulted in a significant increase in body weight gain that was accompanied with a marked increase in energy expenditure as well as a decrease in fasting-induced food intake, with no change in spontaneous food intake. By contrast, when housed at thermoneutrality, *CART*$^{-/-}$ mice showed a reduction in body weight gain compared to controls that was associated with reduced spontaneous and fasting-induced food intake in the absence of any changes in energy expenditure. In line with CART's traditional catabolic role, a lack of CART signaling led to increased adiposity and reduced lean mass at both thermal conditions. A significant upregulation of UCP-1 expression in *CART*$^{-/-}$ mice at RT suggests a critical role of CART signaling for controlling BAT function. This is further supported by in situ hybridization results, demonstrating differential expression profiles of several key hypothalamic neurotransmitters under different thermal conditions, including *TH* in the PVN and *NPY* in the Arc that are known to be critical in BAT-mediated thermoregulation and energy balance control.

The manifestation of differing CART-deficient phenotypes between mice exposed to room temperature versus thermoneutrality indicates the temperature dependence of CART function. For instance, CART signaling has differential effects on weight gain, food intake and energy expenditure under the two temperatures. RT-housed *CART*$^{-/-}$ mice showed markedly accelerated body weight gain occurring on a background of increased energy expenditure without any changes in food intake or physical activity. Increased energy expenditure could represent a secondary effect from the increased body weight gain, where the body attempts to elevate energy dissipation to reduce the energy excess. However, it is also possible that the higher energy expenditure is a compensatory response to the mild cold exposure at 22 °C, consistent with a tendency towards decreased RER, indicating a shift to greater fat oxidation in the knockout mice. Therefore, at RT, CART signaling was implicated in body weight regulation and oxidative fuel selection, yet showed no direct role in modulating food intake and physical activity. In contrast, at TN where cold-induced demand for thermogenesis was eliminated, CART deletion led to reduced body weight gain. It appears that CART signaling has greater impacts on food intake rather than energy expenditure or RER when assessed under an optimal thermoneutral condition. On the other hand, fasting-induced food intake was consistently lower in CART-deficient mice compared to controls under both thermal conditions. This indicates that under an energy deficit state where the orexigenic NPY is expressed at a high level, presence of the anorexigenic CART may still be required to adequately control feeding behavior. We also demonstrated that, despite higher energy expenditure in knockout mice at RT, no difference in body temperature was observed between *CART*$^{-/-}$ and control mice, indicating CART may play a lesser role in regulating whole body temperature, consistent with earlier studies in other *CART* knockout mouse models (Asnicar et al., 2001; Moffett et al., 2006).

Despite the implicated differential roles of CART in the regulation of some metabolic parameters across housing temperatures, *CART*$^{-/-}$ mice consistently demonstrated higher adiposity and lower lean mass at both RT and TN, suggesting an anti-obesogenic function of CART (Asnicar et al., 2001; Moffett et al., 2006). The proportional increase of white adipose deposition within the BAT may at least partially explain the lack of increase in BAT temperature in *CART*$^{-/-}$ mice at the RT condition. BAT weight may not directly reflect BAT thermogenic activity, as the proportion of functional UCP-1 in the total BAT may diminish, hence the absence of significant increases in UCP-1 expression and BAT temperature. PGC-1α and CPT-1 expression levels were not altered by CART deletion at either thermal condition, indicating that CART signaling lacked direct effects on such protein functions. It is also possible that an 8 °C decline in temperature was insufficient to induce activation of the two genes under the current experimental paradigm. Considering that BAT is a highly sympathetically innervated tissue (Lever et al., 1988), the downregulation of *TH* in the PVN as well as the increased Arc *NPY* expression in *CART*$^{-/-}$ mice under mild cold condition showed consistency with the established regulatory circuit by which BAT function is influenced (Shi et al., 2013). Concordantly, comparison of knockouts across temperatures demonstrated that *CART*$^{-/-}$ mice at TN exhibited relatively higher Arc *NPY* level accompanied by reduced PVN *TH* mRNA and lower UCP-1 protein level in BAT. Since Arc *CART* mRNA was increased at TN compared to RT in WT mice, CART function can therefore be seen to oppose NPY effects. Consistent with that, intra-Arc or -PVN injection of CART I (55–102) (Dey et al., 2003; Douglass et al., 1995b) has been reported to stimulate UCP-1 expression and BAT activity in other studies (Kong et al., 2003; Wang et al., 2000), whereas intra-PVN and i.c.v. administration of NPY suppressed brown fat thermogenesis directed through the Arc-PVN neural circuit (Billington et al., 1994; Shi et al., 2013). In sum, the highly coordinated yet complex interactions between CART neurons and other elements in energy metabolism (Barsh and Schwartz, 2002; Schwartz et al., 2000), combined with the potentially confounding effects of mild cold conditioning, may contribute to the dual catabolic/anabolic properties of CART signaling described across studies.

It is also worthy to note that our *CART* knockout mice as well as previously described models (Elefteriou et al., 2005; Gerrits et al., 2011) show a prominent low bone mass phenotype marked by reduced bone mineral density and content when held under RT conditions. Importantly, thermoneutral housing resulted in restoration of bone mass in *CART*$^{-/-}$ mice, suggesting also the temperature-dependence of CART signaling in controlling bone metabolism. The precise mechanism underlying the restoration of bone mass is unclear, although it has been shown that CART inhibits production of the receptor activator of nuclear factor-κB ligand (RANKL) by osteoblasts, which in turn act against bone resorption through reducing osteoclast activity (Elefteriou et al., 2005;

Fig. 4. Expression analysis of key hypothalamic neuropeptides in the regulation of energy metabolism. (A) Temperatures of the interscapular brown adipose tissue and the lumbar back region measured by high-sensitivity infrared imaging in thermoneutral housed WT and *CART*$^{-/-}$ mice at 16 wks of age. (B–G) In situ hybridization for *TH* (B), *CRH* (C), *TRH* (D) mRNA expression at the PVN and *NPY* (E), *AgRP* (F), *POMC* (G) mRNA expression at the Arc in WT and *CART*$^{-/-}$ mice ($n \geq 5$ per group) housed at room temperature (RT) and thermoneutral (TN) conditions. Left: bright-field photomicrographs of coronal brain sections showing mRNA expression for respective genes at the PVN or Arc. Scale bar = 100 μm. Right: hybridization signals are quantified to obtain mean labeling intensity of neurons expressed as percentage coverage of neuronal surface by silver grains (RODs) within the defined areas of interest. 3V, third ventricle; PVN, paraventricular nucleus; Arc, arcuate nucleus; *TH*, tyrosine hydroxylase; *CRH*, corticotropin-releasing hormone; *TRH*, thyrotropin-releasing hormone; *NPY*, neuropeptide Y; *AgRP*, agouti-related protein; *POMC*, proopiomelanocortin. Data are means ± SEM and averaged for all mice from each group examined. $^{*}p \leq 0.05$, $^{**}p \leq 0.01$, $^{***}p \leq 0.001$, $^{****}p \leq 0.0001$ for *CART*$^{-/-}$ versus WT mice or for comparisons between the same genotype across thermal conditions.

Singh et al., 2008). In addition, the interaction between CART and the central NPY system, which is also a known regulator of bone homeostasis and subject to alteration by cold exposure, may also play a role in this process.

Taken together, within the central adaptive system for thermoregulation, CART function is indicated to be regulated in an orchestrated manner through interaction with other neuropeptide pathways implicated with thermoregulatory effects. Substantially, the temperature dependence of CART-deficient traits demonstrated herein reinforces a role of CART in thermoregulation and energy expenditure. However, results from this study also highlight the importance of the temperature dependence of metabolic regulatory systems, hence housing temperature should be taken into consideration when studying aspects of energy homeostasis in mice. Future cross-temperature profiling of the neuropeptides and hormones, that are conjoining general energy homeostasis and thermoregulation pathways, will offer valuable insights into the signaling mechanisms and central sites of action underlying the thermoregulatory impact of CART.

Conflict of interest

No potential conflicts of interest associated with this article were reported and there has been no significant financial support for this work that could have influenced its outcome.

Acknowledgements

We thank the staff of the Garvan Institute Biological Testing Facility for facilitation of the experiments. We are grateful to Dr. Shu Lin for scientific advice, Ronaldo F. Enriquez and Lei Zhai for technical assistance, and Dr. Aitak Farzi for helpful suggestions with the manuscript. This research was supported by the National Health and Medical Research Council of Australia (NHMRC) with a research grant, a Research Fellowship to HH, and a Postgraduate Scholarship to JL.

Appendix A. Supplementary data

Supplementary data to this article can be found online at http://dx.doi.org/10.1016/j.npep.2016.03.006.

References

Asnicar, M.A., Smith, D.P., Yang, D.D., Heiman, M.L., Fox, N., Chen, Y.-F., Hsiung, H.M., Köster, A., 2001. Absence of cocaine- and amphetamine-regulated transcript results in obesity in mice fed a high caloric diet. Endocrinology 142, 4394–4400.

Barsh, G.S., Schwartz, M.W., 2002. Genetic approaches to studying energy balance: perception and integration. Nat. Rev. Genet. 3, 589–600.

Billington, C.J., Briggs, J.E., Harker, S., Grace, M., Levine, A.S., 1994. Neuropeptide Y in hypothalamic paraventricular nucleus: a center coordinating energy metabolism. Am. J. Phys. 266, R1765–R1770.

Bonnefont, J.P., Djouadi, F., Prip-Buus, C., Gobin, S., Munnich, A., Bastin, J., 2004. Carnitine palmitoyltransferases 1 and 2: biochemical, molecular and medical aspects. Mol. Asp. Med. 25, 495–520.

Cannon, B., Nedergaard, J., 2009. Thermogenesis challenges the adipostat hypothesis for body-weight control. Proc. Nutr. Soc. 68, 401–407.

Cannon, B., Nedergaard, J., 2011. Nonshivering thermogenesis and its adequate measurement in metabolic studies. J. Exp. Biol. 214, 242–253.

Challis, B.G., Yeo, G.S., Farooqi, I.S., Luan, J., Aminian, S., Halsall, D.J., Keogh, J.M., Wareham, N.J., O'Rahilly, S., 2000. The CART gene and human obesity: mutational analysis and population genetics. Diabetes 49, 872–875.

Choi, Y.-H., Della-Fera, M.A., Li, C., Hartzell, D.L., Little, D.E., Kuhar, M.J., Baile, C.A., 2004. CART peptide: central mediator of leptin-induced adipose tissue apoptosis? Regul. Pept. 121, 155–162.

del Giudice, E.M., Santoro, N., Cirillo, G., D'Urso, L., Di Toro, R., Perrone, L., 2001. Mutational screening of the CART gene in obese children: identifying a mutation (Leu34Phe) associated with reduced resting energy expenditure and cosegregating with obesity phenotype in a large family. Diabetes 50, 2157–2160.

Dey, A., Xhu, X., Carroll, R., Turck, C., Stein, J., Steiner, D., 2003. Biological processing of the cocaine and amphetamine-regulated transcript precursors by prohormone convertases, PC2 and PC1/3. J. Biol. Chem. 278, 15007–15014.

Dominguez, G., 2006. The CART gene: structure and regulation. Peptides 27, 1913–1918.

Douglass, J., McKinzie, A., Couceyro, P., 1995a. PCR differential display identifies a rat brain mRNA that is transcriptionally regulated by cocaine and amphetamine. J. Neurosci. 15, 2471–2481.

Douglass, J., McKinzie, A., Couceyro, P., 1995b. PCR differential display identifies a rat brain mRNA that is transcriptionally regulated by cocaine and amphetamine. J. Neurosci. 15, 2471–2481.

Elefteriou, F., Ahn, J.D., Takeda, S., Starbuck, M., Yang, X., Liu, X., Kondo, H., Richards, W.G., Bannon, T.W., Noda, M., Clement, K., Vaisse, C., Karsenty, G., 2005. Leptin regulation of bone resorption by the sympathetic nervous system and CART. Nature 434, 514–520.

Elias, C.F., Lee, C.E., Kelly, J.F., Ahima, R.S., Kuhar, M., Saper, C.B., Elmquist, J.K., 2001. Characterization of CART neurons in the rat and human hypothalamus. J. Comp. Neurol. 432, 1–19.

Elmquist, J.K., Maratos-Flier, E., Saper, C.B., Flier, J.S., 1998. Unraveling the central nervous system pathways underlying responses to leptin. Nat. Neurosci. 1, 445–450.

Gerrits, H., Bakker, N.E., van de Ven-de Laat, C.J., Bourgondien, F.G., Peddemors, C., Litjens, R.H., Kok, H.J., Vogel, G.M., Krajnc-Franken, M.A., Gossen, J.A., 2011. Gender-specific increase of bone mass by CART peptide treatment is ovary-dependent. J. Bone Miner. Res. Off. J. Am. Soc. Bone Miner. Res. 26, 2886–2898.

Goossens, G.H., Petersen, L., Blaak, E.E., Hul, G., Arner, P., Astrup, A., Froguel, P., Patel, K., Pedersen, O., Polak, J., Oppert, J.M., Martinez, J.A., Sorensen, T.I., Saris, W.H., 2009. Several obesity- and nutrient-related gene polymorphisms but not FTO and UCP variants modulate postabsorptive resting energy expenditure and fat-induced thermogenesis in obese individuals: the NUGENOB study. Int. J. Obes. 33 (2005), 669–679.

Guerardel, A., Barat-Houari, M., Vasseur, F., Dina, C., Vatin, V., Clement, K., Eberle, D., Vasseur-Delannoy, V., Bell, C., Galan, P., Hercberg, S., Helbecque, N., Potoczna, N., Horber, F., Boutin, P., Froguel, P., 2005. Analysis of sequence variability in the CART gene in relation to obesity in a Caucasian population. BMC Genet. 6, 19.

Hoevenaars, F.P., Bekkenkamp-Grovenstein, M., Janssen, R.J., Heil, S.G., Bunschoten, A., Hoek-van den Hil, E.F., Snaas-Alders, S., Teerds, K., van Schothorst, E.M., Keijer, J., 2014. Thermoneutrality results in prominent diet-induced body weight differences in C57BL/6J mice, not paralleled by diet-induced metabolic differences. Mol. Nutr. Food Res. 58, 799–807.

Joseph-Bravo, P., 2004. Hypophysiotropic thyrotropin-releasing hormone neurons as transducers of energy homeostasis. Endocrinology 145, 4813–4815.

Karp, C.L., 2012. Unstressing intemperate models: how cold stress undermines mouse modeling. J. Exp. Med. 209, 1069–1074.

Kong, W., Stanley, S., Gardiner, J., Abbott, C., Murphy, K., Seth, A., Connoley, I., Ghatei, M., Stephens, D., Bloom, S., 2003. A role for arcuate cocaine and amphetamine-regulated transcript in hyperphagia, thermogenesis, and cold adaptation. FASEB J. 17, 1688–1690.

Kristensen, P., Judge, M.E., Thim, L., Ribel, U., Christjansen, K.N., Wulff, B.S., Clausen, J.T., Jensen, P.B., Madsen, O.D., Vrang, N., Larsen, P.J., Hastrup, S., 1998. Hypothalamic CART is a new anorectic peptide regulated by leptin. Nature 393, 72–76.

Lau, J., Herzog, H., 2014. CART in the regulation of appetite and energy homeostasis. Front. Neurosci. 8.

Lechan, R.M., Fekete, C., 2006. Role of melanocortin signaling in the regulation of the hypothalamic–pituitary–thyroid (HPT) axis. Peptides 27, 310–325.

Lever, J.D., Mukherjee, S., Norman, D., Symons, D., Jung, R.T., 1988. Neuropeptide and noradrenaline distributions in rat interscapular brown fat and in its intact and obstructed nerves of supply. J. Auton. Nerv. Syst. 25, 15–25.

Lodhi, I.J., Semenkovich, C.F., 2009. Why we should put clothes on mice. Cell Metab. 9, 111–112.

Major, G.C., Doucet, E., Trayhurn, P., Astrup, A., Tremblay, A., 2007. Clinical significance of adaptive thermogenesis. Int. J. Obes. 31 (2005), 204–212.

Moffett, M., Stanek, L., Harley, J., Rogge, G., Asnicar, M., Hsiung, H., Kuhar, M., 2006. Studies of cocaine- and amphetamine-regulated transcript (CART) knockout mice. Peptides 27, 2037–2045.

Morrison, Shaun F., Madden, Christopher J., Tupone, D., 2014. Central neural regulation of brown adipose tissue thermogenesis and energy expenditure. Cell Metab. 19, 741–756.

Nicholls, D.G., Locke, R.M., 1984. Thermogenic mechanisms in brown fat. Physiol. Rev. 64, 1–64.

Puigserver, P., Wu, Z., Park, C.W., Graves, R., Wright, M., Spiegelman, B.M., 1998. A cold-inducible coactivator of nuclear receptors linked to adaptive thermogenesis. Cell 92, 829–839.

Ravussin, Y., LeDuc, C.A., Watanabe, K., Leibel, R.L., 2012. Effects of ambient temperature on adaptive thermogenesis during maintenance of reduced body weight in mice. Am. J. Phys. Regul. Integr. Comp. Phys. 303, R438–R448.

Richard, D., Lin, Q., Timofeeva, E., 2002. The corticotropin-releasing factor family of peptides and CRF receptors: their roles in the regulation of energy balance. Eur. J. Pharmacol. 440, 189–197.

Rogge, G., Jones, D., Hubert, G.W., Lin, Y., Kuhar, M.J., 2008. CART peptides: regulators of body weight, reward and other functions. Nat. Rev. Neurosci. 9, 747–758.

Rosen, E.D., Spiegelman, B.M., 2006. Adipocytes as regulators of energy balance and glucose homeostasis. Nature 444, 847–853.

Sainsbury, A., Schwarzer, C., Couzens, M., Herzog, H., 2002. Y2 receptor deletion attenuates the type 2 diabetic syndrome of ob/ob mice. Diabetes 51, 3420–3427.

Scarpace, P.J., Nicolson, M., Matheny, M., 1998b. UCP2, UCP3 and leptin gene expression: modulation by food restriction and leptin. J. Endocrinol. 159, 349–357.

Schwartz, M.W., Woods, S.C., Porte, D., Seeley, R.J., Baskin, D.G., 2000. Central nervous system control of food intake. Nature 404, 661–671.

Shi, Y.-C., Lin, S., Wong, I.P.L., Baldock, P.A., Aljanova, A., Enriquez, R.F., Castillo, L., Mitchell, N.F., Ye, J.-M., Zhang, L., Macia, L., Yulyaningsih, E., Nguyen, A.D., Riepler, S.J., Herzog, H., Sainsbury, A., 2010. NPY neuron-specific Y2 receptors regulate adipose tissue and trabecular bone but not cortical bone homeostasis in mice. PLoS One 5, e11361.

Shi, Y.-C., Lau, J., Lin, Z., Zhang, H., Zhai, L., Sperk, G., Heilbronn, R., Mietzsch, M., Weger, S., Huang, X.-F., Enriquez, R.F., Castillo, L., Baldock, P.A., Zhang, L., Sainsbury, A., Herzog, H., Lin, S., 2013. Arcuate NPY controls sympathetic output and BAT function via a relay of tyrosine hydroxylase neurons in the PVN. Cell Metab. 17, 236–248.

Singh, M.K., Elefteriou, F., Karsenty, G., 2008. Cocaine and amphetamine-regulated transcript may regulate bone remodeling as a circulating molecule. Endocrinology 149, 3933–3941.

Skibicka, K.P., Alhadeff, A.L., Grill, H.J., 2009. Hindbrain cocaine- and amphetamine-regulated transcript induces hypothermia mediated by GLP-1 receptors. J. Neurosci. 29, 6973–6981.

Small, C.J., Kim, M.S., Stanley, S.A., Mitchell, J.R.D., Murphy, K., Morgan, D.G.A., Ghatei, M.A., Bloom, S.R., 2001. Effects of chronic central nervous system administration of agouti-related protein in pair-fed animals. Diabetes 50, 248–254.

Speakman, J.R., Krol, E., 2005. Limits to sustained energy intake IX: a review of hypotheses. J. Comp. Physiol. B. 175, 375–394.

Swoap, S.J., Li, C., Wess, J., Parsons, A.D., Williams, T.D., Overton, J.M., 2008. Vagal tone dominates autonomic control of mouse heart rate at thermoneutrality. Am. J. Physiol. Heart Circ. Physiol. 294, H1581–H1588.

Vrang, N., 2006. Anatomy of hypothalamic CART neurons. Peptides 27, 1970–1980.

Vrang, N., Larsen, P.J., Clausen, J.T., Kristensen, P., 1999a. Neurochemical characterization of hypothalamic cocaine-amphetamine-regulated transcript neurons. J. Neurosci. 19, RC5.

Vrang, N., Tang-Christensen, M., Larsen, P.J., Kristensen, P., 1999b. Recombinant CART peptide induces c-Fos expression in central areas involved in control of feeding behaviour. Brain Res. 818, 499–509.

Vrang, N., Larsen, P.J., Kristensen, P., Tang-Christensen, M., 2000. Central administration of cocaine-amphetamine-regulated transcript activates hypothalamic neuroendocrine neurons in the rat. Endocrinology 141, 794–801.

Wang, C.F., Billington, C.J., Levine, A.S., Kotz, C.M., 2000. Effect of CART in the hypothalamic paraventricular nucleus on feeding and uncoupling protein gene expression. Neuroreport 11, 3251–3255.

Wierup, N., Richards, W.G., Bannon, A.W., Kuhar, M.J., Ahrén, B., Sundler, F., 2005. CART knock out mice have impaired insulin secretion and glucose intolerance, altered beta cell morphology and increased body weight. Regul. Pept. 129, 203–211.

Yamada, K., Yuan, X., Otabe, S., Koyanagi, A., Koyama, W., Makita, Z., 2002. Sequencing of the putative promoter region of the cocaine- and amphetamine-regulated-transcript gene and identification of polymorphic sites associated with obesity. Int. J. Obes. 26, 132–136.

Yanik, T., Dominguez, G., Kuhar, M.J., Del Giudice, E.M., Loh, Y.P., 2006. The Leu34Phe ProCART mutation leads to cocaine- and amphetamine-regulated transcript (CART) deficiency: a possible cause for obesity in humans. Endocrinology 147, 39–43.

Zhou, Q.Y., Quaife, C.J., Palmiter, R.D., 1995. Targeted disruption of the tyrosine hydroxylase gene reveals that catecholamines are required for mouse fetal development. Nature 374, 640–643.